ACCEPTED FOR PUBLICATION IN APJ LETTERS, APRIL 7, 2011
Preprint typeset using LaTeX style emulateapj v. 11/10/09

PIERCING THE GLARE: A DIRECT IMAGING SEARCH FOR PLANETS IN THE SIRIUS SYSTEM*

C. THALMANN[1,2], T. USUDA[3], M. KENWORTHY[4], M. JANSON[5], E. E. MAMAJEK[6], W. BRANDNER[2], C. DOMINIK[1,7], M. GOTO[2], Y. HAYANO[3], T. HENNING[2], P. M. HINZ[8], Y. MINOWA[3], M. TAMURA[9]

Accepted for publication in ApJ Letters, April 7, 2011

ABSTRACT

Astrometric monitoring of the Sirius binary system over the past century has yielded several predictions for an unseen third system component, the most recent one suggesting a $\lesssim$50 $M_{\rm Jup}$ object in a $\sim$6.3-year orbit around Sirius A. Here we present two epochs of high-contrast imaging observations performed with Subaru IRCS and AO188 in the 4.05 μm narrow-band Br α filter. These data surpass previous observations by an order of magnitude in detectable companion mass, allowing us to probe the relevant separation range down to the planetary mass regime (6–12 $M_{\rm Jup}$ at 1″, 2–4 $M_{\rm Jup}$ at 2″, and 1.6 $M_{\rm Jup}$ beyond 4″). We complement these data with one epoch of M-band observations from MMT/AO Clio, which reach comparable performance. No dataset reveals any companion candidates above the 5 σ level, allowing us to refute the existence of Sirius C as suggested by the previous astrometric analysis. Furthermore, our Br α photometry of Sirius B confirms the lack of an infrared excess beyond the white dwarf's blackbody spectrum.

Subject headings: planetary systems — techniques: high angular resolution — stars: individual (Sirius A) — stars: individual (Sirius B) — white dwarfs

1. INTRODUCTION

One and a half centuries ago, Sirius was found to host a faint binary companion (Bond 1862). The orbital motion of this pair has been monitored ever since, leading to a number of publications that claimed to find periodic perturbations indicative of the presence of an unseen third system component, Sirius C. The most recent analysis predicted a substellar companion in a $\sim$6.3-year circumstellar orbit around Sirius A (Benest & Duvent 1995, and references therein). While the amplitude of the purported astrometric signal, 56 mas, would suggest a companion mass of 72 $M_{\rm Jup}$, these authors imposed an upper limit of $\lesssim$ 50 $M_{\rm Jup}$ on the basis of system stability considerations. Since no measure of confidence is given, we assume a conservative lower limit of half the measured amplitude, 28 mas, on the basis of their plotted periodograms, resulting in a minimal mass of 36 $M_{\rm Jup}$.

This would place Sirius C in the so-called brown dwarf desert, the range of orbital parameter space around stars in which brown dwarfs are found to be scarce (e.g. Marcy & Butler 2000; Grether & Lineweaver 2006). Numerical simulations of the formation and evolution of brown dwarf companions reproduce this scarcity, regardless of the formation process assumed (e.g. as part of the star formation process (Bate & Bonnell 2005), planet formation by core accretion (Mordasini et al. 2009) or gravitational fragmentation (Stamatellos & Whitworth 2009)), thus these rare objects impose important constraints on theory.

However, Sirius' extreme brightness – both apparent and absolute – had long thwarted attempts to verify these claims through direct imaging. Kuchner & Brown (2000) established first constraints on substellar companions at separations of 1.″5–3″ with space-based coronography at 1.02 μm on HST NICMOS, whereas Bonnet-Bidaud & Pantin (2008) used ground-based observations assisted by adaptive optics on ESO ADONIS to achieve similar constraints in the range of 3″–10″. These limits left most of the parameter space in which Sirius C was expected unexplored. In this work, we present new results from 4.05 μm observations on Subaru IRCS as well as from M-band observations on MMT/AO Clio, which improve the companion mass constraints by an order of magnitude and extend the coverage down to an inner working angle of 0.″7. With a baseline of 4.3 years among the observations, the chance that a companion be missed in all datasets due to adverse geometric conditions is slim.

Sirius A is an A1V-type star at a distance of 2.64 pc, a mass of 2.02 $M_\odot$ and an age of 225–250 Myr, whereas Sirius B is a white dwarf of 0.98 $M_\odot$ with a cooling age of 124 $\pm$ 10 Myr orbiting Sirius A with a 50-year period (e.g. Liebert et al. 2005). The combination of youth and extreme proximity (cf. a median target distance of 22 pc in the Gemini Deep planet survey, Lafrenière et al. 2007b) allow us to explore unusually small orbital radii, with planetary-mass detection limits down to separations of 2.5 AU in projection.

2. OBSERVATIONS

The Sirius system was observed with the Subaru IRCS instrument (Kobayashi et al. 2000) on January 20, 2011, using the AO188 adaptive optics system (Hayano et al. 2010). The Br α narrow-band filter at 4.05 μm was chosen, since this band has been shown both theoretically and observationally to provide the best combination of PSF quality and brightness contrast for planet detection in the speckle-dominated regime (Janson et al. 2008, 2009, 2010). The dataset consists of 56 frames, each comprising 240 co-adds of 0.1 s exposures, for a total integration time of 22.4 min. Although IRCS does not offer Lyot coronography, a mirror plate with several circular

* Based on data collected at Subaru Telescope, which is operated by the National Astronomical Observatory of Japan, and at the MMT Observatory, a joint facility of the University of Arizona and the Smithsonian Institution.

[1] Anton Pannekoek Astronomical Institute, University of Amsterdam, The Netherlands; thalmann@uva.nl.
[2] Max Planck Institute for Astronomy, Heidelberg, Germany.
[3] Subaru Telescope, Hilo, Hawai'i, USA.
[4] Leiden Observatory, Leiden University, P.O. Box 9513, 2300 RA Leiden, The Netherlands.
[5] University of Toronto, Toronto, Canada.
[6] University of Rochester, Rochester NY, USA.
[7] Radboud University, Nijmegen, The Netherlands.
[8] University of Arizona, Tucson AZ, USA.
[9] National Astronomical Observatory of Japan, Tokyo, Japan.

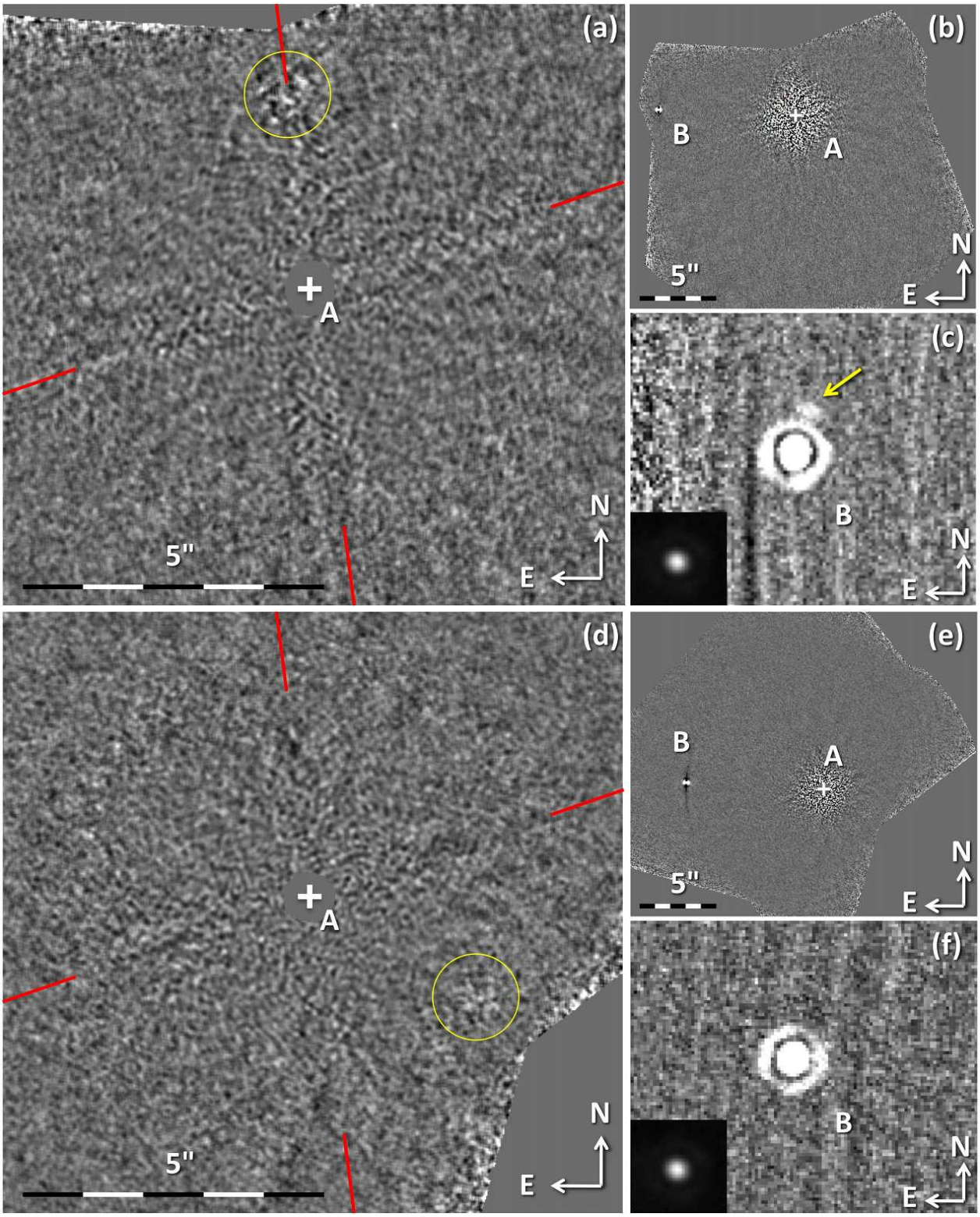

FIG. 1.— (a–c) Results of the January 2011 ADI observations of the Sirius system in the Br α band with Subaru IRCS. (a) Signal-to-noise map of the inner $\sim 10'' \times 10''$, calculated in concentric annuli after convolution with a 4 px diameter circular aperture. The stretch is $[-5\,\sigma, 5\,\sigma]$. The location of Sirius A is marked with a white plus sign. The short red lines indicate the position angles where residuals of the spider diffraction pattern slightly elevate the noise level. The yellow circle marks the area of increased noise generated by one of the unused mirror holes in the field of view. (b) Full field of view of the ADI intensity image. Sirius B is visible to the East of Sirius A. (c) Non-differential image of Sirius B. Unsharp masking on the scale of 15 pixels ($3\,\lambda/D$) has been applied to reduce background structures. The point source just outside Sirius B's first Airy ring is a ghost caused by a filter. The cutout shows Sirius B's unsaturated PSF core. (d–f) The corresponding images for the March 2011 Subaru IRCS data.

holes is available to reject light from the primary star. We used a hole with a projected radius of 0.″3 to avoid excessive saturation; nevertheless, the shoulders of Sirius A's point-spread function (PSF) locally saturate out to a radius of ∼0.″6. The plate scale was 20 mas per pixel.

Follow-up observations were taken with Subaru IRCS on March 12, 2011. Using the same observing strategy, 83 frames were taken for 33.2 min of total integration time.

Furthermore, we make use of M-band imaging data taken on December 5, 2006, with the Clio 3–5 μm imager (Freed et al. 2004) in conjunction with the adaptive secondary mirror on the 6.5 m MMTO telescope (Brusa et al. 2004). The star was nodded 5.″5 along the long axis of the detector after five images were taken. Each of the 322 images consists of 50 co-added exposures of 209.1 ms length, for a total co-added duration of 56.1 min. To avoid variations in the pattern of illumination on the Clio detector, the instrument is fixed in orientation with respect to the telescope, resulting in total field rotation of 24.6° for our Sirius data. Conditions were photometric, and the seeing 0.″5–0.″7 (as seen with the video rate optical acquisition camera) at an air mass of 1.50–1.64. The plate scale was 49 mas per pixel.

All observations were taken in pupil-stabilized image orientation to enable the angular differential imaging technique (ADI, Marois et al. 2006). We employed the LOCI algorithm (Locally Optimized Combination of Images, Lafrenière et al. 2007a) in order to search for faint point sources in Sirius A's speckle halo. This form of ADI is the most powerful high-contrast imaging method currently available, as evidenced by recent direct detections of substellar companions (e.g. Thalmann et al. 2009; Marois et al. 2010) and even circumstellar disks (Thalmann et al. 2010; Buenzli et al. 2010). We employed the LOCI parameters described as optimal for the test dataset in Lafrenière et al. (2007a), with a frame selection criterion of 0.5 FWHM to avoid self-subtraction of companion signals. Given the excellent resulting image quality, we refrained from further parameter fine-tuning. In all datasets, the inner working angle of 0.″7 is due to detector nonlinearity and saturation rather than insufficient field rotation.

3. RESULTS

3.1. *Subaru IRCS Br α Data*

The final Br α images after ADI reduction are presented in Figures 1a–f. No obvious point-sources around Sirius A are visible. To confirm this numerically, we first convolve the image with a sampling aperture of 4 pixel diameter, and then calculate the signal-to-noise map (S/N) by dividing the pixel values in concentric annuli around the star by their standard deviation. As expected, we find no signal above the $5\,\sigma$ level, discounting the locally elevated noise in the shadow of the unused mirror holes.

We do find a conspicuous signal in the immediate vicinity of Sirius B in the January 2011 data (Figure 1c). However, closer inspection of the signal's behavior in the time-series of images reveals it to be locked to the position angle of the pupil rather than the field, and identifies it as a ghost. No such signal is seen in the March 2011 data. Apart from this, the environs of Sirius B are background-limited outside the first Airy ring.

We use the unsaturated PSF of Sirius B in the Br α images for photometric calibration. Although no prior Br α photometry of Sirius B exists, its overall brightness in the near- to mid-infrared can be predicted by a $25{,}193 \pm 37$ K blackbody (Barstow et al. 2005; Skemer & Close 2011). Model spectra by Lejeune et al. (1997) for a range of $\log g$ values up to 5 cm/s^2 for $T_{\rm eff} = 25{,}000$ K indicate that while absorption lines are present in the mid-infrared, they exhibit rather small equivalent width. For the Br α absorption line we estimate an equivalent width of 0.7 nm, and hence conclude that it does not present a significant deviation from a blackbody.

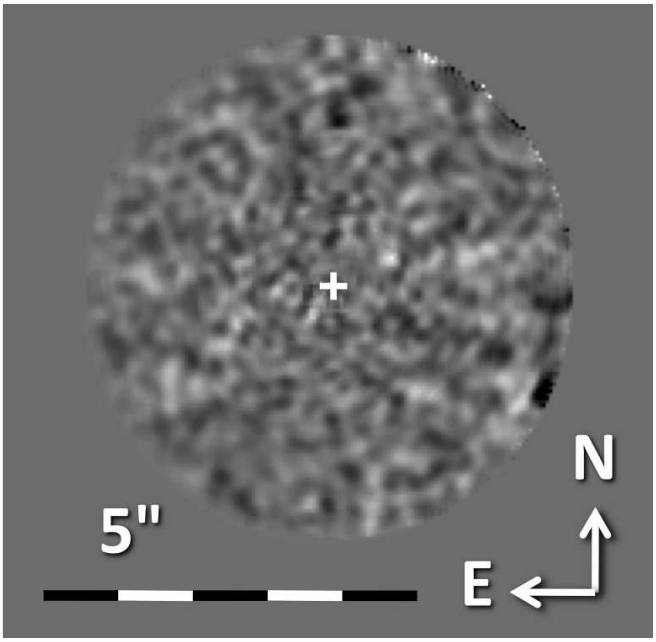

FIG. 2.— Signal-to-noise map of the inner $4'' \times 4''$ of the MMT/AO Clio M-band data. The stretch is $[-5\,\sigma, 5\,\sigma]$. No significant signal is found.

As an independent confirmation, we calibrate Sirius B's brightness using a brief observation of the A1V-type star HD 40138 as a reference. The result, 9.27 ± 0.17 mag, is consistent with our expected value of 9.17 ± 0.10 mag, which is based on the J-band photometry by Bonnet-Bidaud & Pantin (2008) and stellar spectra by Castelli & Kurucz (2003). This provides further evidence that Sirius B does not have an infrared excess from circumstellar dust as proposed by Bonnet-Bidaud & Pantin (2008).

3.2. *MMT/AO Clio M-band data*

Individual images from Clio are beam-subtracted, and a sigma clipping routine is used to remove hot pixels deviating by more than $3\,\sigma$ from a 5×5 pixel region centered on that pixel. The location of the central star is estimated by smoothing the images with a Gaussian kernel with FWHM 10 pixels and estimating the location of the resultant peak. All the science images are then passed into a LOCI data reduction pipeline (Lafrenière et al. 2007a). The LOCI processing carries out reduction in 4 pixel (0.″2) wide rings starting from an inner radius of 4 pixels (0.″2). Each optimization section extends 20 pixels beyond the outer radius of the current ring, ensuring that the optimization section contains the equivalent area of a minimum of 150 PSF cores. After the LOCI background subtraction is performed, the resultant images are rotated into the frame of the sky before being averaged together to give a final output image.

Again, no significant signal above the $5\,\sigma$ threshold is found. The S/N map is shown in Figure 2.

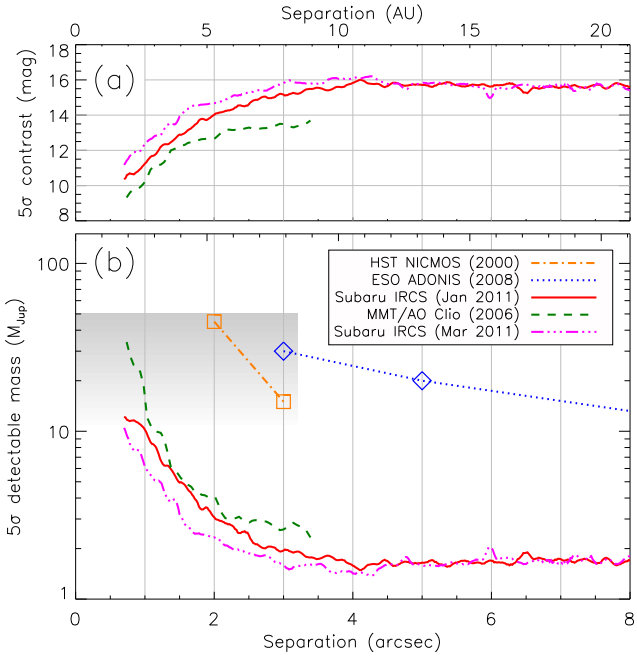

FIG. 3.— Limits on faint companions to Sirius A. (a) Effective $5\,\sigma$ detectable contrast to Sirius A in the January 2011 Br α data, (solid red), the M-band data (dashed green), and the March 2011 Br α data (dash-dot-dot-dotted magenta) as a function of separation, corrected for partial subtraction. (b) The companion masses corresponding to those contrasts, derived according to an updated version of the method of Janson et al. (2008) from the COND evolutionary model (Allard et al. 2001; Baraffe et al. 2003). For comparison, the constraints established by Kuchner & Brown (2000, dash-dotted orange) and Bonnet-Bidaud & Pantin (2008, dotted blue) are overplotted. The gray shaded area indicates the parameter space of a $\lesssim$50 $M_{\rm Jup}$ companion in a 6.3-year orbit (semi-major axis $a = 1\farcs6$).

3.3. *Contrast and detectable companion mass*

The $5\,\sigma$ contrast curves established by the three datasets is presented in Figure 3. The partial self-subtraction of point sources during the LOCI reduction is estimated by inserting artificial $10\,\sigma$ point sources into the raw data across the entire usable range of separations from the star, and retrieving their surviving flux after subjecting them to the LOCI pipeline (radial filtering and optimized background subtraction). The plotted curves are corrected for this flux loss and therefore represent effective detectable contrast. The process is described in detail in Lafrenière et al. (2007a, Section 4.3.).

The COND-based evolutionary models (Allard et al. 2001; Baraffe et al. 2003) are used to convert the M-band brightness contrast into detectable mass. For the Br α data, we adopt an updated version of the method used in Janson et al. (2008). COND model spectra (Allard et al. 2001) are used to re-calculate photometric predictions from COND-based evolutionary models (Baraffe et al. 2003) from L' band to the IRCS Br α band, for masses of 1–20 $M_{\rm Jup}$ and the age of the Sirius system (250 Myr). The measured brightness contrast as function of angular separation is then translated into detectable mass, using these values.

The Br α data are sensitive to masses in the planetary regime down to the inner working angle of $0\farcs7$ around Sirius A (6–10 $M_{\rm Jup}$ at 1″, 2–3 $M_{\rm Jup}$ at 2″), and reach 1.6 $M_{\rm Jup}$ in the thermal background beyond 4″, which includes the immediate surroundings of Sirius B down to $0\farcs2$. The M-band data achieve comparable performance in a more restricted field of view ($<3\farcs5$).

4. DISCUSSION

Our high sensitivity to substellar companions around Sirius A allows the first thorough test of the hypothesis of a $\lesssim$50 $M_{\rm Jup}$ body, "Sirius C", in a 6.3-year orbit around Sirius A as proposed by Benest & Duvent (1995). As these authors point out, though, a single negative detection does not prove the non-existence of such an object. Even though the semi-major axis of such an orbit is $a = 4.3$ AU, corresponding to $1\farcs6$ at the distance of 2.64 pc, both projection effects and eccentricity can leave the companion at an apparent separation below the inner working angle of $0\farcs7$ at the time of observation.

To quantify the likelihood of a false negative result, we systematically calculate the projected orbital ellipses for 6.3-year orbits with eccentricities $e = \{0, 0.04, \ldots, 0.96\}$ and arguments of periastron $\omega = \{0°, 10°, \ldots, 350°\}$. Since we make use of radial detectable mass curves (Fig. 3), we are insensitive to the orbit's overall position angle on sky; thus no variation of the longitude of the ascending node Ω is necessary. As for the inclination, we explore two scenarios: The coplanar case, where Sirius C shares the orbital plane of the Sirius AB system with an inclination of 136.6°, and the free case, where all system orientations on the unit sphere are considered equally likely, resulting in a statistical weight of $\sin i$ for each inclination $i = \{0°, 1°, \ldots, 90°\}$. The mass of Sirius C is sampled as $m = \{0.5, 1, \ldots, 20\}\ M_{\rm Jup}$.

On each ellipse, 1000 possible companion positions at the epoch of our M-band observations are chosen, with uniform spacing in eccentric anomaly. We then calculate the corresponding location at the epoch of the other two datasets. The detectable mass curves are evaluated to determine whether or not the companion would have been detected at $\geq 5\,\sigma$ at least once in that configuration. For each ellipse, the detection likelihood is averaged over all companion positions, whereby a statistical weight is assigned to each position to account for the non-uniform evolution of eccentric anomaly with time. The weight is proportional to the time that the companion spends at each position over the course of an orbit, approximated by half the distance to the two adjacent positions in the sequence divided by the local orbital velocity. Finally, the detection likelihoods are averaged over all i and ω to yield the detection completeness for each combination of eccentricity e and companion mass m. The results of this analysis are plotted in Figure 4.

We find that coplanar companions down to 6 $M_{\rm Jup}$ can be excluded at the $5\,\sigma$ level at 100% completeness. The completeness remains above 50% down to 2–3.5 $M_{\rm Jup}$, depending on eccentricity. If no constraints are imposed on the inclination, edge-on orbits emerge that can hide Sirius C behind Sirius A's glare. As a result, the completeness values for masses above 12 $M_{\rm Jup}$ drop to 97–99% for certain eccentricity ranges, and down to 90% for masses of 5–7 $M_{\rm Jup}$.

The astrometric signal reported by Benest & Duvent (1995), 56 mas, implies a companion mass of 72 $M_{\rm Jup}$. The authors furthermore impose an upper mass limit of $\lesssim$50 $M_{\rm Jup}$ on the basis of system stability considerations. While no lower mass limit is given, we derive a conservative estimate of half that value, 36 $M_{\rm Jup}$, from their published periodograms. Given our much lower detection limits, our three combined epochs of high-contrast imaging can therefore decisively reject their Sirius C hypothesis.

Although Benest & Duvent (1995) provide no error estimation, we consider a false alarm the most likely explana-

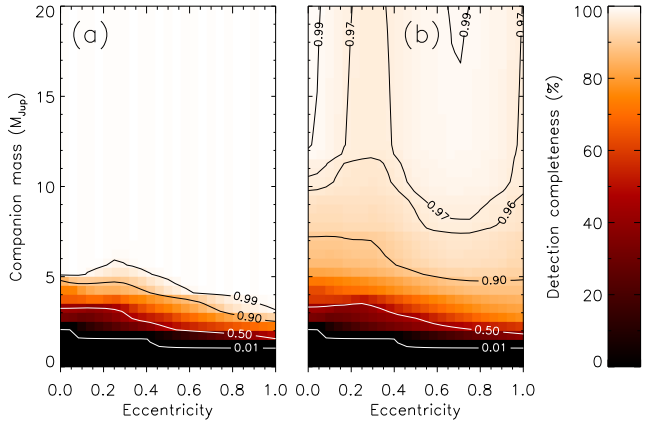

FIG. 4.— Probability of at least one $5\,\sigma$ detection of a companion with a 6.3-year orbit around Sirius A in our three datasets, as a function of companion mass m and eccentricity e. (a) The case of coplanar orbits with the Sirius AB system (inclination $i = 136.6°$). All companions above $6\,M_{\rm Jup}$ can be rejected regardless of orbital phase (100% completeness). The completeness remains above 50% down to 2–3.5 $M_{\rm Jup}$ depending on eccentricity. (b) If the inclination is unconstrained ($p(i) \propto \sin i$), edge-on orbits become possible, introducing a chance of a few percent that Sirius C might elude detection in all observations. Nevertheless, our three datasets provide decisive evidence against the existence of Sirius C as proposed by Benest & Duvent (1995).

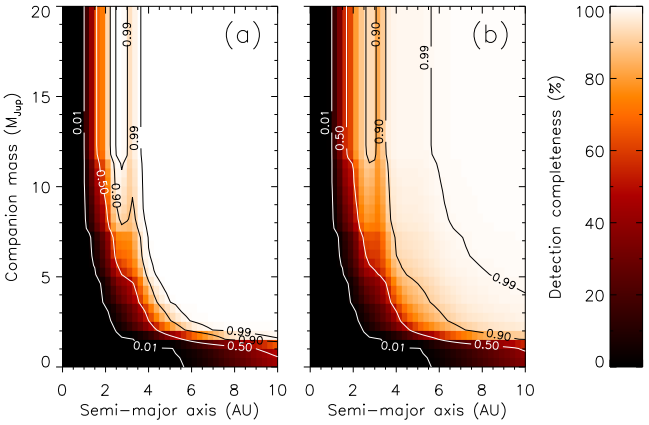

FIG. 5.— Probability of at least one $5\,\sigma$ detection of a companion around Sirius A in our three datasets, as a function of companion mass m and semi-major axis a. A flat distribution in eccentricities is assumed. (a) The case of coplanar orbits with the Sirius AB system (inclination $i = 136.6°$). (b) The case of unconstrained inclination ($p(i) \propto \sin i$). The false negative probability is large for the stable planet orbit regime at $a \lesssim 2\farcs17$ (Holman & Wiegert 1999).

tion for their results. Precision astrometry is known to suffer from a multitude of systematic errors (e.g. subtle changes in pixel scale and orientation, and differential atmospheric refraction which depends on airmass, parallactic angle, and ambient conditions), and has led to a series of spurious detections in the past (e.g. Pravdo & Shaklan (2009) vs. Bean et al. (2010) and Lazorenko et al. (2011); van de Kamp (1969) vs. Gatewood & Eichhorn (1973)).

Leaving astrometric predictions aside, we can also explore the parameter space for other semi-major axes. Figure 5 shows the completeness as a function of semi-major axis $a = \{0.25,\ 0.50,\ \ldots,\ 10.0\}$ AU and companion mass m, assuming a flat distribution in eccentricity. Although our data are sensitive to planets down to an inner working angle of $0\farcs7$ and down to $1.6\,M_{\rm Jup}$ at large separations, the completeness values drop quickly at shorter separations (e.g. 50% for a $10\,M_{\rm Jup}$ object at $a = 2$ AU). This coincides with the domain of long-term stable planet orbits predicted by Holman & Wiegert (1999), with a critical semi-major axis $a_{\rm c} = 2.17$ AU. Therefore, plenty of parameter space remains for unseen planets around Sirius A. The upcoming next generation of high-contrast instruments, such as SPHERE (Beuzit et al. 2010), will offer smaller inner working angles and better contrast performance, and thus stand a good chance to detect such planets. In particular, due to its extreme proximity and brightness, Sirius is the third most promising target (after α Centauri A and B) for the direct detection of exoplanets in reflected light with the SPHERE ZIMPOL imaging polarimeter (Thalmann et al. 2008).

One thing to keep in mind is the fact that Sirius B was originally a $\sim 5\,M_\odot$ progenitor star that expanded into a supergiant $\sim$125 Myr ago, with potentially dramatic consequences for the system architecture (Liebert et al. 2005). Accretion of ejected material from Sirius B may have caused planets around Sirius A to gain mass and heat, migrate, or form in the first place as second-generation planets (e.g. Perets 2010). Since these processes would leave the planets hotter and brighter than their unperturbed 250 Myr-old counterparts, our detectable planet mass curves in Figure 3 are conservative for such objects.

5. CONCLUSIONS

We present three high-contrast imaging datasets of the Sirius system, all of which reach detection performances in the planetary regime (6–12 $M_{\rm Jup}$ at $1''$, 2–4 $M_{\rm Jup}$ at $2''$, 1.6 $M_{\rm Jup}$ beyond $4''$). This constitutes an improvement of an order of magnitude in detectable planet mass. Taken up to 4.3 years apart, the observations allow us to refute the existence of a substellar companion with a mass of $\lesssim$50 $M_{\rm Jup}$ in a 6.3-year orbit as predicted from astrometry measurements of the Sirius AB system (Benest & Duvent 1995). For a companion mass above 12 $M_{\rm Jup}$, the chances of a triple false negative at a $5\,\sigma$ threshold are 0–4%, depending on eccentricity. For the special case of coplanar orbits, the probability is 0% down to $6\,M_{\rm Jup}$). However, we note that our observations leave open the possibility for Jupiter- and Neptune-sized planets around Sirius A, especially at short angular separations.

Furthermore, we confirm the absence dust around Sirius B by the lack of an infrared excess at 4.05 μm within our precision of 0.17 mag.

We thank David Lafrenière for generously having provided us with the source code for his LOCI algorithm. We are grateful for the privilege of observing from Mauna Kea, which holds great cultural significance for the Hawai'ian indigenous community.

Facilities: Subaru (IRCS, AO188), MMT/AO (Clio).

REFERENCES

Allard, F., Hauschildt, P. H., Alexander, D. R., Tamanai, A., & Schweitzer, A. 2001, ApJ, 556, 357

Baraffe, I., Chabrier, G., Barman, T. S., Allard, F., & Hauschildt, P. H. 2003, A&A, 402, 701

Barstow, M. A., Bond, H. E., Holberg, J. B., Burleigh, M. R., Hubeny, I., & Koester, D. 2005, MNRAS, 362, 1134

Bate, M. R., & Bonnell, I. A. 2005, MNRAS, 356, 1201

Bean, J. L., Seifahrt, A., Hartman, H., Nilsson, H., Reiners, A., Dreizler, S., Henry, T. J., & Wiedemann, G. 2010, ApJ, 711, L19
Benest, D., & Duvent, J. L. 1995, A&A, 299, 621
Beuzit, J.-L., et al. 2010, Astronomical Society of the Pacific Conference Series, 430, 231
Bond, G. 1862, Astronomische Nachrichten, 57, 131
Bonnet-Bidaud, J. M., & Pantin, E. 2008, A&A, 489, 651
Brusa, G., Miller, D. L., Kenworthy, M. A., Fisher, D. L., & Riccardi, A. 2004, Proc. SPIE, 5490, 23
Buenzli, E., et al. 2010, A&A, 524, L1
Castelli, F., & Kurucz, R. L. 2003, Modelling of Stellar Atmospheres, 210, 20P
Freed, M., Hinz, P. M., Meyer, M. R., Milton, N. M., & Lloyd-Hart, M. 2004, Proc. SPIE, 5492, 1561
Gatewood, G., & Eichhorn, H. 1973, AJ, 78, 769
Grether, D., & Lineweaver, C. H. 2006, ApJ, 640, 1051
Hayano, Y., et al. 2010, Proc. SPIE, 7736, 77360N
Holman, M. J., & Wiegert, P. A. 1999, AJ, 117, 621
Janson, M., Reffert, S., Brandner, W., Henning, T., Lenzen, R., & Hippler, S. 2008, A&A, 488, 771
Janson, M., et al. 2009, MNRAS, 399, 377
Janson, M., Bergfors, C., Goto, M., Brandner, W., & Lafrenière, D. 2010, ApJ, 710, L35
Kobayashi, N., et al. 2000, Proc. SPIE, 4008, 1056
Kuchner, M. J., & Brown, M. E. 2000, PASP, 112, 827
Lafrenière, D., Marois, C., Doyon, R., Nadeau, D., & Artigau, É. 2007, ApJ, 660, 770
Lafrenière, D., et al. 2007, ApJ, 670, 1367
Lazorenko, P. F., et al. 2011, A&A, 527, A25
Lejeune, T., Cuisinier, F., & Buser, R. 1997, A&AS, 125, 229
Liebert, J., Young, P. A., Arnett, D., Holberg, J. B., & Williams, K. A. 2005, ApJ, 630, L69
Marcy, G. W., & Butler, R. P. 2000, PASP, 112, 137
Marois, C., Lafrenière, D., Doyon, R., Macintosh, B., & Nadeau, D. 2006, ApJ, 641, 556
Marois, C., Zuckerman, B., Konopacky, Q. M., Macintosh, B., & Barman, T. 2010, Nature, 468, 1080
Mordasini, C., Alibert, Y., & Benz, W. 2009, A&A, 501, 1139
Perets, H. B. 2010, arXiv:1001.0581
Pravdo, S. H., & Shaklan, S. B. 2009, ApJ, 700, 623
Skemer, A. J., & Close, L. M. 2011, arXiv:1101.4314
Stamatellos, D., & Whitworth, A. P. 2009, MNRAS, 392, 413
Thalmann, C., et al. 2008, Proc. SPIE, 7014,
Thalmann, C., et al. 2009, ApJ, 707, L123
Thalmann, C., et al. 2010, ApJ, 718, L87
van de Kamp, P. 1969, AJ, 74, 757